

# Phase Composition and Tribological Characteristics of the Surface Layers of Carbon Tool Steels after Laser Processing in Air

A. V. Sidashov<sup>a</sup>, A. T. Kozakov<sup>b, \*</sup>, S. I. Yaresko<sup>c, \*\*</sup>, N. G. Kakovkina<sup>c</sup>, and D. S. Manturov<sup>a</sup>

<sup>a</sup>Rostov State Transport University, Rostov-on-Don, 344038 Russia

<sup>b</sup>Research Institute of Physics, Southern Federal University, Rostov-on-Don, 344090 Russia

<sup>c</sup>Lebedev Physical Institute, Samara Branch, Russian Academy of Sciences, Samara, 443011 Russia

\*e-mail: kozakov\_a@mail.ru

\*\*e-mail: yarsi54@gmail.com

Received April 15, 2020; revised June 17, 2020; accepted June 20, 2020

**Abstract**—We present the results of studies of the phase composition of an oxide layer formed on the surface of U8 and U10 carbon tool steels after laser treatment in air using a quasi-continuous laser source. Data on the structure of the oxide–metal interfaces are obtained by X-ray photoelectron spectroscopy using the  $AlK_{\alpha,1,2}$  line; the SPECS surface analysis system is applied. The thickness of the completely oxidized surface layers is 38.7 and 99.0 nm, respectively, for steels U8 and U10. The thickness of the transition layer (81.0 nm) located at the interface with unmodified bulk steel and consisting of iron oxide FeO and iron atoms for U10 steel is approximately two times smaller than that for U8 steel. We determine the composition of the oxides on the surface of the steels after laser processing. The surface of U8 steel is mainly a wustite film, the presence of which determines the poor wear characteristics of the surface of the laser-action zone. On the contrary, the thicker oxide layer of modified U10 steel containing  $Fe_2O_3$  and  $Fe_3O_4$  with better strength characteristics ensures a higher wear resistance of the U10 steel surface after laser processing during tribological tests. For U10 steel, the wear rate of the modified surface is more than halved, while for U8 steel, this figure is only ~17%.

**Keywords:** laser processing, surface, X-ray photoelectron spectroscopy, oxidized surface layers, elemental composition, phase composition, tribological testing

**DOI:** 10.1134/S1027451021010316

## INTRODUCTION

Laser action, depending on the parameters and methods of treatment, gaseous medium, elemental composition, and the methods of the bulk heat treatment of steels, has a multifactorial effect on the state of their surface and near-surface layers, which is the subject of numerous studies [1–4]. Along with the methods of laser modification [1–4], the laser texturing of a surface using various technological schemes and methods of direct laser processing (LP) [5–9] is also effective in improving the tribological properties of materials. The method is successfully applied for structural materials [5–7], including ceramics (for example, based on silicon carbide [6, 7]), and ensures a decrease in the coefficient of friction and an increase in the performance characteristics of machine parts and mechanisms.

One of the significant results of laser action, which is not associated with a change in the surface microrelief, is the formation of a thin oxide film on the surface of steel during laser processing in air. Studies of the kinetics of heating metals and analysis of the growth,

structure, and optical properties of oxide layers formed when metals are heated by laser radiation (LR) made it possible to clarify the physical concepts of the thermal-chemical mechanisms of the interaction of intense laser radiation with matter [10–13] and make significant progress in understanding the occurring metal-oxidation processes.

Studying the effect of laser radiation on the kinetics of the formation of oxide films on the surface of alloy steels (AISI 329 (analogue of 08Cr5N4M2 steel), AISI 304 (analog of 08Cr18N10 steel), 9CrC, R6M5, steel 45, etc.) has demonstrated that depending on the elemental composition of steels, both the thickness of the films and the phase composition over the thickness of the film change, as well as the ratio between iron oxides of various valences and oxides of alloying elements [14–20]. The effect of laser treatment in air on the behavior of a cutting tool made of heat-resistant steels of the R9K5 type is expressed, first of all, in an increase in the stability of the surface properties of the laser-irradiated zone (LIZ) when cutting in the tool–part contact zone [21]. Laser treatment in air not only stabilizes the process of tool wear and minimizes the

wear rate but also leads to significant expansion of the range of cutting conditions at which its least wear is achieved.

The range of thicknesses of oxide films formed on bulk metal substrates when they are heated without melting by a laser pulse of millisecond duration is quite wide: from cover films (<0.1 nm, for chromium and tantalum) to rather thick films (~100 nm, for titanium and steels) [22]. Upon exposure to continuous laser radiation, the thickness of oxide films can reach tens of micrometers [23] and more. Metal oxide films with a thickness of 100–200 nm play an essential role in reducing the coefficient of friction in the contact zone [21, 24–28], lowering the intensity of the stress field on tool working surfaces, decreasing the temperature and force load on the cutting wedge, and increasing tool life [3, 28]. It is generally accepted that the formation of protective oxide formations prevents severe wear and decreases friction [26, 27]. The intensity of this phenomenon depends on the thickness and composition of the oxide layers. The effect of films on the wear of metal-cutting tools is multifactorial. According to Usmanov and Yakunin [26], surface films can also cause metal hardening due to the suppression of surface sources of dislocations and due to dissolution of a part of the film in highly deformed surface layers and the subsequent blocking of dislocations by “Cottrell atmospheres.” The “barrier effect” of the film, as well as of the hardened surface layer, depends on the temperature–rate conditions of deformation. The secondary structures of the surface of the laser-irradiated zone in the form of oxide films, along with a structurally modified layer extending down to a depth of 900  $\mu\text{m}$  (and deeper in some cases), affect the performance characteristics of steels of various compositions, purposes, structures, including carbon tool steels [4, 29–31].

In this regard, it is of interest to study the phase composition of iron oxides on a laser-irradiated surface and its distribution over the thickness in a thin surface oxide layer formed by laser radiation of the same power, not only in heat-resistant tool steels [15, 16] but also in carbon tool steels, differing in content by the presence of just one element (carbon). These are carbon steels U8 and U10, which are widely used in the manufacture of tools operating under conditions that do not cause heating of the cutting edge and some wear-resistant parts. These steels are most often used for the manufacture of metrological tools for controlling the shape and dimensions of parts and tools (for example, calipers for various purposes). The quality of manufacturing calipers is subject to increased requirements for manufacturing accuracy, wear resistance, and constancy of the working dimensions. Laser treatment is an effective method for maintaining the high wear resistance of the surface layers of these steels and meeting the above requirements.

The goal of this work is to study the structure and phase composition of thin oxide films of the laser-irradiated surface of tool carbon steels U8 and U10 and to analyze the depth distribution of the structural components of oxides and their effect on the tribological characteristics of the LIZ surface.

## EXPERIMENTAL

The laser treatment of samples of steels U8 and U10 with dimensions of  $10 \times 10 \times 1.5$  mm was carried out using an LK-150/1500-QCW-AC fiber-optic ytterbium quasi-continuous laser source with a wavelength of 1.07  $\mu\text{m}$ . The laser power was 130 W; the processing speed was 3 mm/s. In all experiments, the pulse-repetition rate was 25 kHz with a single pulse duration of 20  $\mu\text{s}$ . The irradiation modes were selected in such a way as to exclude surface melting. The laser beam moved along the surface of the sample parallel to one of the sides, forming stripes 0.6–0.8 mm wide; the distance between the centers of the stripes was ~0.4–0.5 mm. As a result, the entire irradiated region of the sample was a uniform structure. The appearance of the sample surface after laser processing is presented in Fig. 1a, and the corresponding SEM image is given in Fig. 1b.

Ion profiling of the samples was carried out in the pretreatment chamber of the SPECS surface analysis system. An ion gun was attached to the flange of the pretreatment chamber in such a way that ion-beam irradiation was carried out strictly vertically. Profiling with  $\text{Ar}^+$  ions was carried out for 10–13 h with an interval of 5–10 min with the following parameters of ion-gun operation:  $I_{\text{acc}} = 2.99$  keV, beam current  $I = 10$  mA, and the argon pressure was no more than  $4.5 \times 10^{-3}$  Pa.

Qualitative and quantitative analysis of the chemical composition of the surface and near-surface layers of the samples of tool carbon steels was carried out by X-ray photoelectron spectroscopy (XPS) using a surface analysis system (SPECS, Germany). An  $\text{AlK}_{\alpha}$  monochromated X-ray line with an energy of 1486.6 eV was used as the excitation radiation.

The energy resolution of the analyzer was 0.45 eV for the  $\text{Ag}3d_{3/2}$  line. We used the carbon  $\text{C}1s$  line as an external standard for determining the binding energies; the energy of the line was taken to be 285 eV. The pressure in the vacuum chamber during measurement was maintained at a level of  $8 \times 10^{-8}$  Pa.

Microstructural analysis was performed using cross sections. To reveal the structure of the base metal and the structure of the laser-action zone, we used a 4% solution of  $\text{HNO}_3$  in ethyl alcohol. Metallographic analysis was performed using a Neophot-30 optical microscope (Carl Zeiss) and an EVO 50 EP scanning electron microscope at a magnification from 100 to 14000 times.

Tribological studies were carried out using an Anton Paar tribometer Model 6.2.8 in the linear

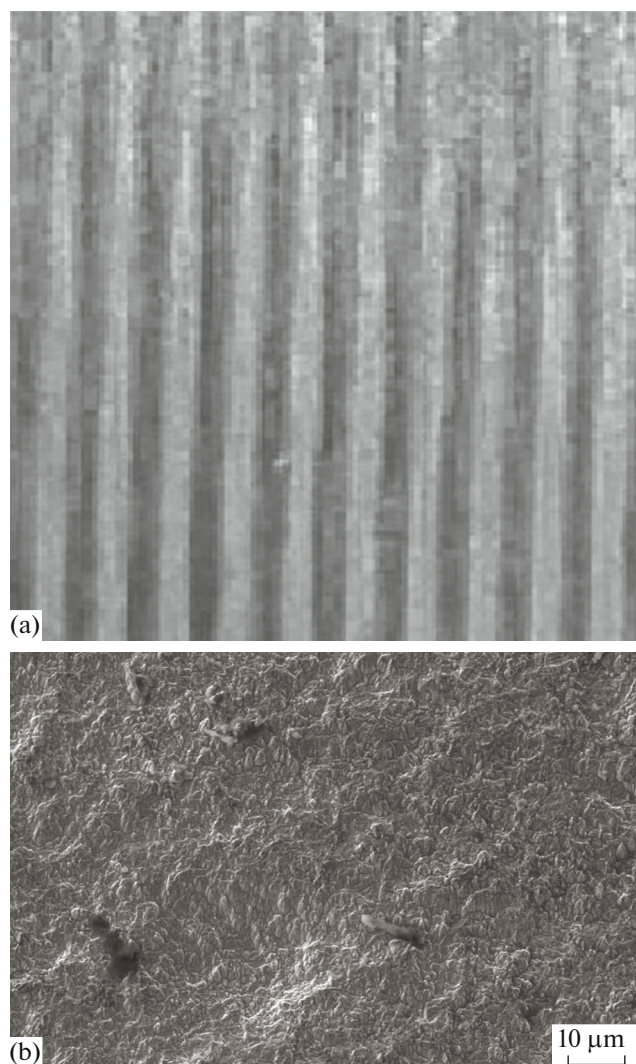


**Fig. 1.** Surface of the sample (U8 steel) after laser processing: (a) appearance,  $\times 5$ ; (b) SEM image of the surface microrelief.

motion mode under ambient conditions at 50% relative humidity. The total amplitude of the reciprocating motion was 1 mm; the vibrational frequency was 10 Hz at a vertical load of 5 N. The counterbody was a ball 6 mm in diameter, made of corundum  $\text{Al}_2\text{O}_3$ .

#### *Fe2p, O1s, and C1s XPS Spectra of the Laser-Irradiated Surface of Steels U8 and U10*

The spectra of internal  $2p$  levels of iron atoms for steels U8 and U10 (Figs. 2 and 3, respectively) were obtained at different times of ion profiling of the surface after laser treatment. The spectra were recorded every 5 min during the first hour of etching, and then at an interval of 10 min until the oxygen concentration dropped to less than 7 at %. Figures 2 and 3 do not show all those spectra, the profiles of which demon-

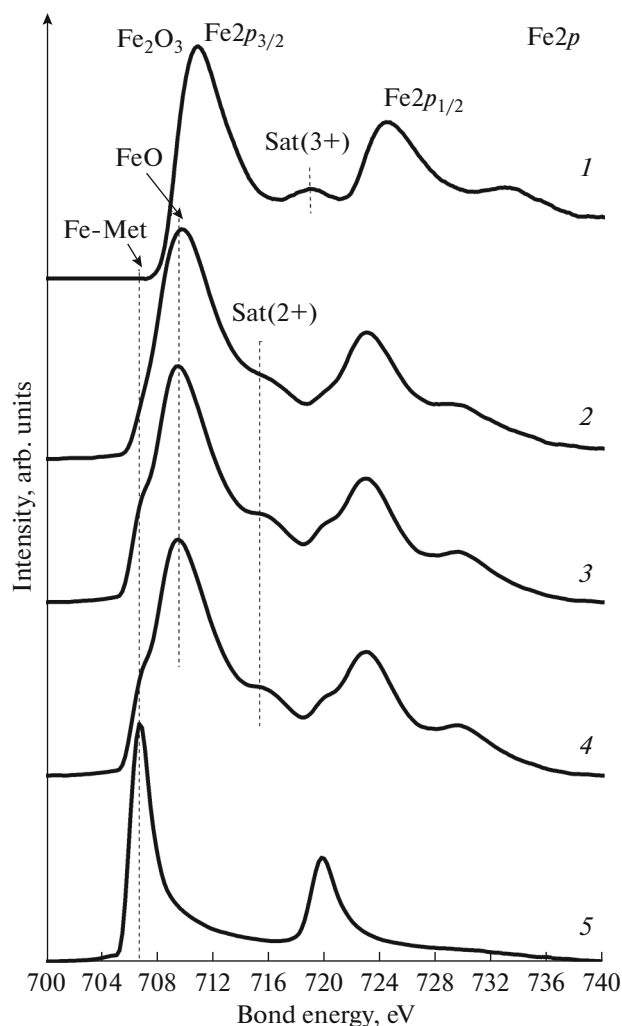


**Fig. 2.** Fe2p XPS spectra recorded after etching the laser-irradiated zone of U8 steel: (1) initial surface, (2) 30 min, and (3) 4, (4) 9, and (5) 12 h.

strate the most significant details of the iron-oxidation process.

The Fe2p spectra (Figs. 2 and 3) consist mainly of two peaks:  $\text{Fe}2p_{3/2}$  and  $\text{Fe}2p_{1/2}$ , which correspond to the emission of an electron from the  $2p_{3/2}$  and  $2p_{1/2}$  levels of iron, separated by spin-orbit interaction. In addition to these main lines, the spectra contain details of the fine structure, which are indicated in Figs. 2 and 3 by vertical dashed lines. These lines belong to the so-called charge-transfer satellites Sat. (+2) and Sat. (+3), by which it is easy to identify whether an iron ion is in the bivalent or trivalent state [16, 32]. The energy position of the  $\text{Fe}2p_{3/2}$  and  $\text{Fe}2p_{1/2}$  peaks serves as an additional feature that makes it possible to distinguish whether iron is in an oxidized state or not and also to determine the oxidation state itself.

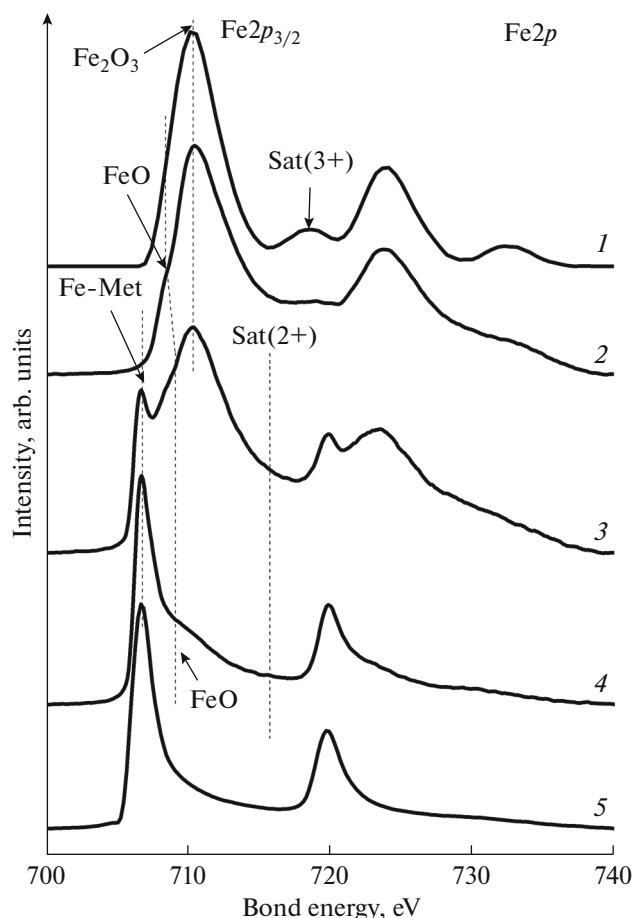


**Fig. 3.** Fe2p XPS spectra recorded after etching the laser-irradiated zone of U10 steel: (1) initial surface, (2) 4, (3) 7, (4) 9, and (5) 10 h.

The component of the Fe2p<sub>3/2</sub> level, having an energy in the range of 706.7–707.8 eV, refers to unoxidized iron [33, 34]. The component of the Fe2p<sub>3/2</sub> level with an energy in the range of 710.3–710.7 eV belongs to Fe<sub>3</sub>O<sub>4</sub>, the component with the energy in the range of 711.0–711.5 eV is for Fe<sub>2</sub>O<sub>3</sub>, and the component with an energy of 709.5 eV is for FeO. An additional sign of the presence of magnetite Fe<sub>3</sub>O<sub>4</sub> in the layer under study is the presence in the profile of the Fe2p<sub>3/2,1/2</sub> spectrum of a characteristic feature with energy spaced from the spectrum maximum at a distance of 1.8 eV towards lower binding energies and the absence of a charge transfer satellite Sat. (+3) with an energy of approximately 718.5 eV [32, 35].

Considering the above, we note that iron ions on the surface of the samples of U8 and U10 steels, formed by laser treatment, and in the layers below are in different oxidized states. A more detailed analysis shows that the distributions of chemical bonds of iron with oxygen over the depth of the oxidized iron layer in U8 and U10 steels, determined from the energy position and fine structure of the Fe2p<sub>3/2,1/2</sub> spectra, are

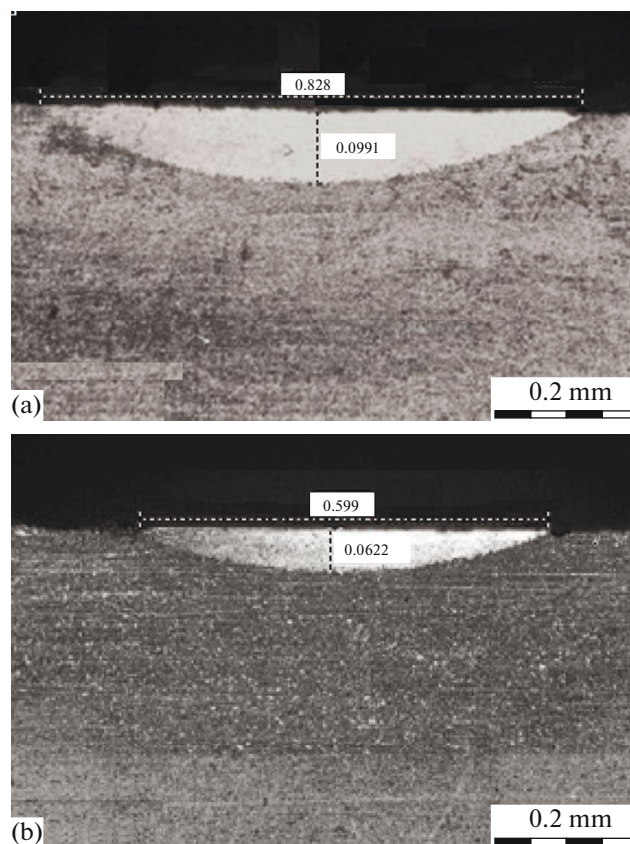


**Fig. 4.** Cross section of the laser-irradiated zone for (a) steel U8 and (b) steel U10.

not identical (Figs. 2 and 3), although these steels are analogous. The Fe-Me component, which indicates the presence of iron in the metal state in the test layer, appears after etching for 4 h for U8 steel and 6 h for U10 steel. This may be an indicator of a greater thickness of the oxide layer on the laser-irradiated surface of U10 steel compared to U8 steel. The depth of the laser-irradiated zone with the modified structure after laser treatment for U10 steel (~100 μm) is also greater than that for U8 steel (~60 μm) (Fig. 4).

Figure 5 shows the O1s X-ray photoelectron spectra obtained at the surface and over the depth of the U8 and U10 steels after laser processing. Near the surface, the X-ray photoelectron spectra of oxygen of both plates of steel (Fig. 5, spectrum 4 for U8 steel and spectrum 8 for U10 steel) have three components: A, B, and C. Component A has an energy in the range of 529.9–530.2 eV. This component can be attributed to the oxygen of one of the iron oxides (for the iron oxides detected on the surfaces of both plates of steel, the energy of the O1s line changes insignificantly) [33, 34]. We attribute component B at an energy of ~531.7–531.9 eV to adsorbed oxygen and component C at an energy in the range of 533.1–534.0 eV to water oxygen and/or a hydroxyl group [32, 33].

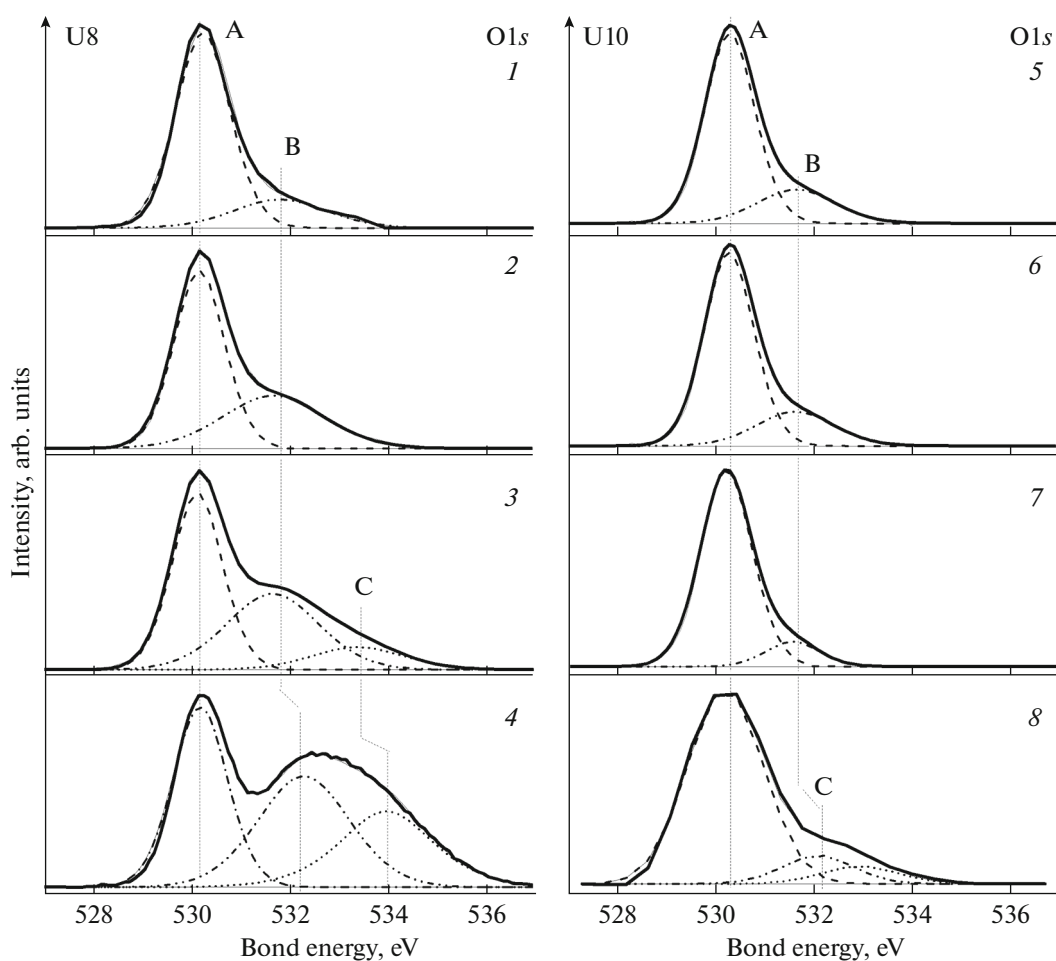


**Fig. 5.** O1s XPS spectra recorded after etching the laser-irradiated zone of (left) U8 steel and (right) U10 steel: (1) 8, (2) 4, (3) 15 min, (4) initial surface, (5) 10, (6) 6, (7) 3 h, and (8) initial surface.

Subsequently, as atoms of the surface elements are etched off the surface, only two components remain in the oxygen spectrum: component A, which is related to iron oxide, and component B (of low intensity), which is related to adsorbed oxygen. Further etching fails to remove component B completely. Consequently, it can refer to either oxygen dissolved in steels or oxygen located at grain boundaries in steels.

Figure 6 shows the C1s X-ray photoelectron spectra obtained at the surface and depth of the laser-irradiated zone of U8 steel.

On the initial surface, carbon is in one state corresponding to hydrocarbon contamination with  $E_b = 285$  eV (component A). Component A' refers to carbon bonds with OH groups. During ion etching, while component A related to hydrocarbon contamination remains in the carbon spectrum, component B appears at an energy of approximately 283.0 eV. This component can be attributed to the carbide structural component of steels, which is present in the quenching zone after laser treatment, according to the data of metallographic analysis.

Already after 20 min of ion etching, the total amount of fixed carbon (from contamination and bound to the metal of the alloy) in the analyzed surface layer becomes significantly smaller. At a depth corresponding to 9 and 13 h of ion etching, the carbon concentration decreases to approximately 0.2 at %. The change in the C–H spectrum over the depth of U10 steel is similar. It has two components on the surface, related to hydrocarbon contamination with  $E_b = 285$  eV (main) and the bonds of carbon with OH groups (low intensity). As the main component disappears, a component with a binding energy of about 283.0 eV begins to appear, which we attribute to the carbide structural component of steels.

#### *Phase Composition of Oxide Layers over the Laser-Irradiated Depth for U8 and U10 Steels*

The distributions of the concentrations of iron, oxygen, and carbon over the depth of oxide layers formed on the laser-irradiated surface of U8 and U10 steels are shown in Figs. 7a and 7b, respectively.

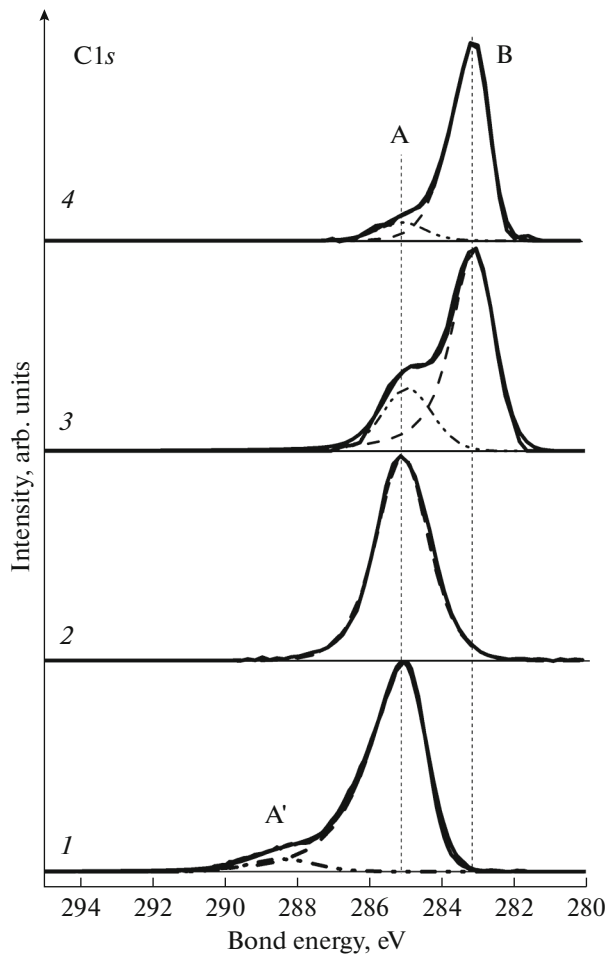


**Fig. 6.** C1s XPS spectra recorded after etching the laser-irradiated zone of U8 steel: (1) initial surface, (2) 30 min, and (3) 9 and (4) 13 h.

Comparison of the presented data indicates a difference in the formed oxide layers on the surface of both plates of steel already at the stage of studying the concentration dependences over depth. Carbon and oxygen on the surface are represented by surface contamination typical of steels exposed to the environment; although their concentration can also be affected by the carbon contained in the steels or, more correctly, the enrichment of the surface with it under the action of laser radiation. Their concentrations are also determined by the type of oxide formed under high-speed laser heating. In the shallowest surface layer, the concentrations of carbon, oxygen, and iron for U8 and U10 steels are 63, 32, and 4 at % (Fig. 7a) and 40, 46, and 14 at % (Fig. 7b), respectively. The concentration of carbon and oxygen decreases with depth for both plates of steel. For U8 steel, the carbon concentration becomes close to the bulk one (3.5 at %) only at a depth corresponding to 2 h of ion etching, and for U10 steel, the carbon concentration sharply

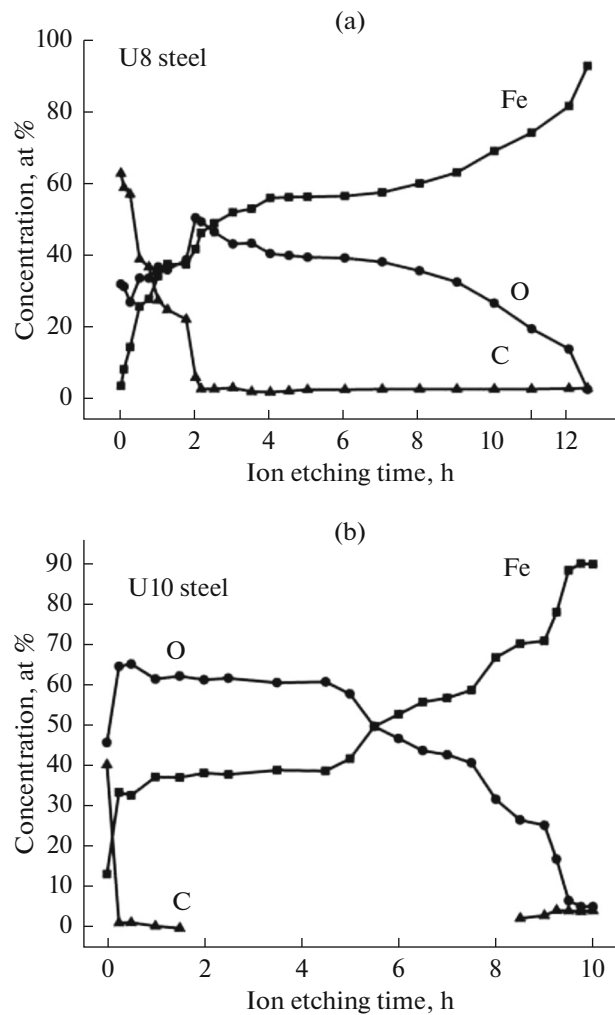


**Fig. 7.** Concentrations of elements over depth depending on the time of ion etching after laser processing for (a) U8 steel and (b) U10 steel.

decreases and becomes the same as the bulk one already at a depth corresponding to 0.3 h of ion etching.

The oxygen concentration in U8 steel coincides with the iron concentration after the removal of surface contaminants in terms of carbon and oxygen, from 1 to 2 h of ion etching (Fig. 7a), which may indicate the formation of an FeO compound in this layer. After 2 h of etching, the oxygen concentration in the studied oxide layer gradually decreases, remaining smaller than the iron concentration, which indicates a change in the oxidation state of iron over the depth of the oxide layer. The behavior of the concentration dependences for iron and oxygen for U10 steel differs in comparison with those for U8 steel. After the removal of surface contaminants to the etching point of 5.5 h, the oxygen concentration exceeds the iron concentration by 1.6 times. This value is close to the ratio of the oxygen and iron concentrations in Fe<sub>2</sub>O<sub>3</sub> oxide.

For a more accurate assessment of the chemical states of iron, the Fe2p spectra of iron of U8 and U10 steels, recorded during the entire etching time over the depth of the oxide layer, were decomposed into components corresponding to a certain iron valence. The decomposition procedure is described in [16, 32]. Figures 8a and 8b show the results of this decomposition, the analysis of which makes it possible to refine significantly the data presented in Figs. 7a and 7b.

The study of the distribution of iron oxides over the depth of the oxide layers after laser processing shows that on the surface of both plates of steel, iron atoms are in two oxidized states, Fe<sup>2+</sup> and Fe<sup>3+</sup>, indicating the presence of two oxides, FeO and Fe<sub>2</sub>O<sub>3</sub> (Figs. 8a and 8b). For U8 steel, the layer in which FeO and Fe<sub>2</sub>O<sub>3</sub> coexist is rather thin. However, for U10 steel, the surface layer containing FeO and Fe<sub>2</sub>O<sub>3</sub> extends deep up to 2 h of ion etching.

For U8 steel, the oxide layer appears to consist only of iron in the oxidized state Fe<sup>2+</sup> after 15 min of etching and up to 2 h (inclusive), which is consistent with the data of Fig. 7a. The surface state corresponding to the etching time interval between 2 and 2.5 h is represented by a thin layer of Fe<sub>3</sub>O<sub>4</sub>. Starting from 2.5 h of etching, pure iron and iron in the Fe<sup>2+</sup> oxidation state appear for the first time at the studied depth.

U10 steel also has a thin layer of Fe<sub>3</sub>O<sub>4</sub> located above the layer where pure iron is detected by XPS. Under a layer of the composition Fe<sub>3</sub>O<sub>4</sub>, there is a layer consisting of a mixture of FeO and iron in the zero oxidation state, that is, Fe-Me, in which the concentration of FeO gradually decreases, and the concentration of iron Fe<sup>0</sup> increases until it becomes the same as the concentration of iron in the bulk of the steel.

## RESULTS AND DISCUSSION

Laser treatment of both types of steels led to modification of their phase composition at depths of up to 100 μm, which is in agreement with the published data [1–4]. Of particular interest is the analysis of changes in a thin surface layer, associated with the formation of laser-induced secondary oxide structures of the laser-irradiated surface. The factors that determine the change in the structure of steels on the laser-irradiated surface differ from the factors that determine its change over the depth of the heat-affected zone. In the former case, metal heated above the temperature of phase transformations could interact with atmospheric oxygen. The surface layers of the metal were oxidized to form oxides of various stoichiometry, the chemical composition, thickness, and relative position of which are shown in Figs. 8a and 8b for U8 and U10 steels, respectively.

Although the concentration curves (Fig. 7a) and the curves characterizing the phase composition of the oxides (Figs. 8a and 8b) quantitatively differ from each

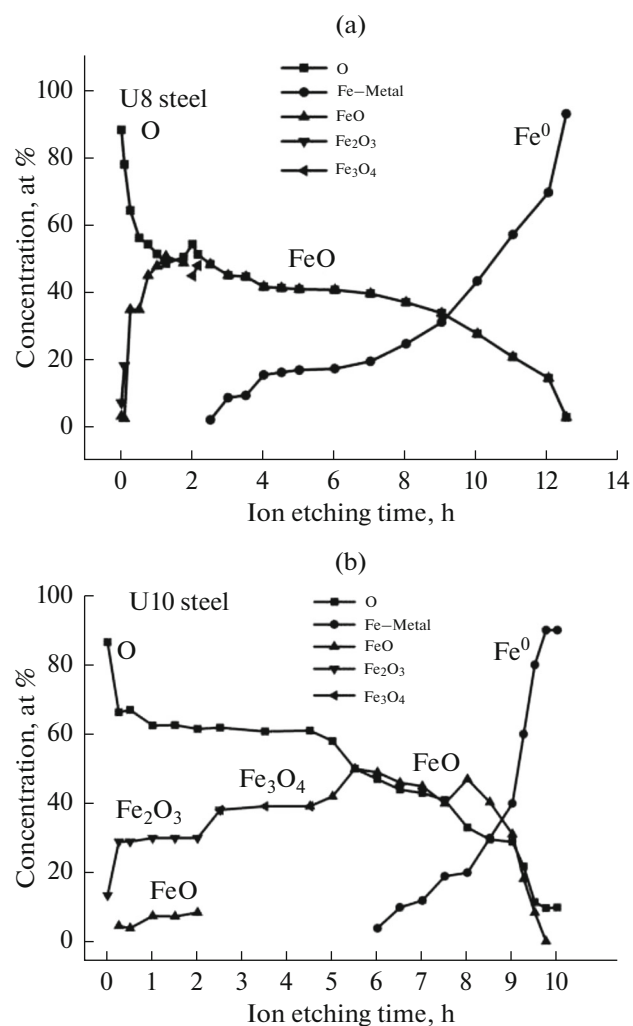


**Fig. 8.** Distribution of iron oxides over the depth of oxide layers after laser processing in (a) U8 steel and (b) U10 steel.

other, the qualitative pattern of the oxidation of steels under laser treatment is approximately the same. Based on the data of Fig. 8, we schematically present the relative position and thickness of various oxides on U8 and U10 steels (Fig. 9).

It is rather difficult to find the absolute depths of the oxide layers: they depend on many factors [33] and are determined by the operation time of the ion gun, the density of the ion beam, etc. According to the data obtained earlier [16], the rate of ion etching of steels using the used ion gun is ~0.3 nm/min. The uncertainty of the above ion etching rate in depth profiling is approximately 1%. Using this value and the known time of passage of oxide layers (for example, Fig. 8) during ion etching, we determined the thicknesses of oxide layers in U8 and U10 steels discussed below.

In both steel plates, the surface layer consists of FeO and Fe<sub>2</sub>O<sub>3</sub> (Figs. 8 and 9). For U8 steel, this layer of a mixture of oxides is rather thin (1.5 nm), which

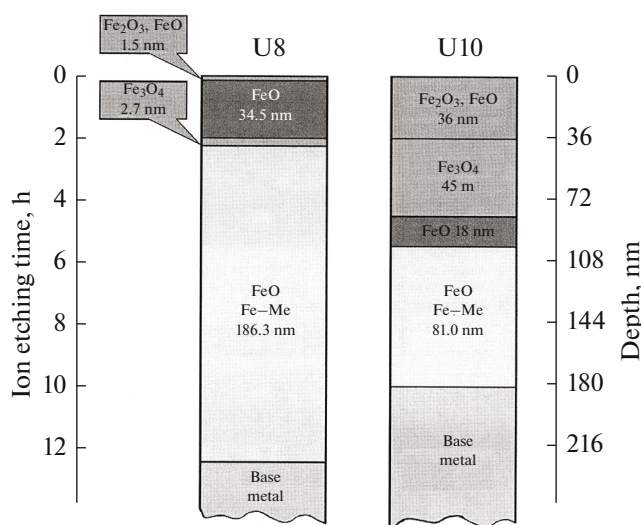


Fig. 9. Arrangement and thickness of oxide layers on the surface of U8 and U10 steels.

practically coincides with the depth of XPS analysis. For U10 steel, this layer is much thicker and reaches 36.0 nm. For U8 steel, the mixture of FeO and Fe<sub>2</sub>O<sub>3</sub> is replaced with increasing depth by a layer of FeO (34.5 nm), directly behind which there is a thin layer of oxide of the composition Fe<sub>3</sub>O<sub>4</sub> (2.7 nm). The latter is adjacent to a layer (186.3 nm) consisting of a mixture of FeO and iron atoms Fe<sup>0</sup> (Fig. 9). The total thickness of oxides on the surface of steel U8 is only 38.7 nm, but together with the transition layer of FeO and Fe<sup>0</sup> at the boundary with the steel base, the thickness of the oxidized layer of U8 steel can be estimated to be 225.0 nm.

Qualitatively, the arrangement of oxides on the surface of U10 steel does not differ from that for U8 steel, but there is a quantitative difference in the thicknesses of the oxide layers with the same phase composition (Fig. 9). For example, the layer of the composition Fe<sub>3</sub>O<sub>4</sub> of U10 steel is significantly thicker and amounts to 45.0 nm. The FeO layer of U10 steel is below the Fe<sub>3</sub>O<sub>4</sub> layer and has a thickness of 18.0 nm. It borders with a transition layer located at the interface with the unmodified bulk steel U10 and a layer consisting of FeO and iron atoms Fe<sup>0</sup> with a thickness that is approximately two times smaller than that of U8 steel and amounts to 81.0 nm. The thickness of only oxides on the surface of U10 steel is more than twice that of U8 steel and is 99.0 nm. However, the total thickness of the oxide layer of U10 steel together with the transition layer of FeO and atoms Fe<sup>0</sup> at the boundary with the steel base is somewhat smaller compared to the total thickness of the oxide layer of U8 steel and amounts to 180.0 nm.

The determined arrangement of the oxide layers formed under conditions of high-speed laser heating correlates quite well with the mutual arrangement of

the oxide layers obtained by high-temperature isothermal oxidation [36].

The most significant difference between oxidation under conditions of laser heating and isothermal heating is that the rate of laser oxidation depends not only on the target temperature but also on the intensity of the incident laser radiation [37]. The total diffusion flux, which is the driving force of oxidation, is determined not only by the term proportional to the concentration gradient (this flux leads to Wagner's law [36]) but also by the term proportional to the temperature gradient, the value of which is mainly determined by the thermal EMF coefficient of the oxide ( $\alpha$ ). For thermal EMF values of less than zero (for example,  $\alpha = -430 \mu\text{V}/\text{deg}$  for Fe<sub>3</sub>O<sub>4</sub> and  $-500 \mu\text{V}/\text{deg}$  for FeO, while for  $\alpha = 380 \mu\text{V}/\text{deg}$  Fe<sub>2</sub>O<sub>3</sub> [38]), the oxidation rate decreases with an increase in the radiation intensity, and thermal-diffusion processes do not affect the rate of laser oxidation. Therefore, we can assume that the process of the formation of FeO and Fe<sub>3</sub>O<sub>4</sub> obeys the Wagner parabolic law, that is,

$$dx/dt = k_n' / 2x,$$

where  $k_n'$  is the oxidation-rate constant [36], which describes the processes associated with the concentration gradient. For Fe<sub>3</sub>O<sub>4</sub>,  $k_n' = 1.05 \times 10^{-2} \exp(-40500/RT)$  cm<sup>2</sup>/s, and for FeO,  $k_n' = 5.75 \times 10^{-2} \exp(40500/RT)$  cm<sup>2</sup>/s.

Assuming that the oxide layers on iron grow parabolically and proportionally, let us estimate the thickness of the iron-oxide films, for example, a Fe<sub>3</sub>O<sub>4</sub> film on U10 steel. According to estimates, for the experimentally obtained parameters of the laser-irradiated zone (Fig. 4b), the characteristic time of action of the laser source to achieve the required depth of the hardened layer is  $\sim 1.5$  ms. At a surface temperature of 15–20% less than the melting temperature of steel, which corresponds to the real conditions of the experiment, we obtained a thickness for the Fe<sub>3</sub>O<sub>4</sub> film, limited by diffusion processes, of 34.6–48.5 nm, which is in good agreement with the experimental data.

The estimates also correlate well with the thicknesses of the oxide layers formed on the surfaces of alloyed tool steel 9CrC and high-speed tool steel R6M5 after pulsed laser processing [3, 16] and are consistent with the results of calculations [22], according to which rather thick ( $\sim 100$  nm) oxide films are formed on bulk metals and steels upon heating without melting by a millisecond pulse.

#### TRIBOLOGICAL CHARACTERISTICS OF SURFACE OXIDES IN THE LASER-IRRADIATED ZONE

To assess the effect of the oxide-phase composition of the laser-irradiated surface, obtained on U8 and



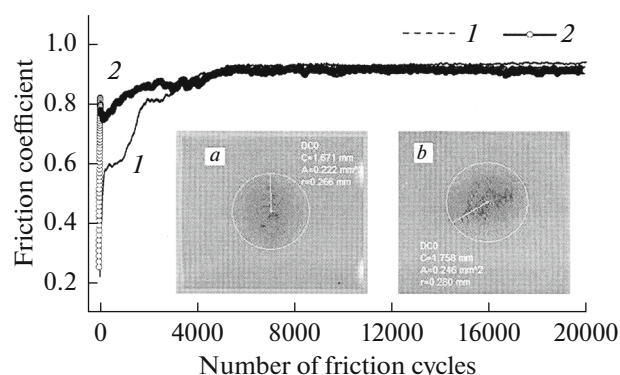


**Fig. 10.** Coefficients of friction depending on the distance traveled for (1) the modified and (2) the initial surface of U8 steel. Inset: images of the wear trace on the surface of the test ball when sliding along (a) the modified and (b) initial surfaces, respectively.

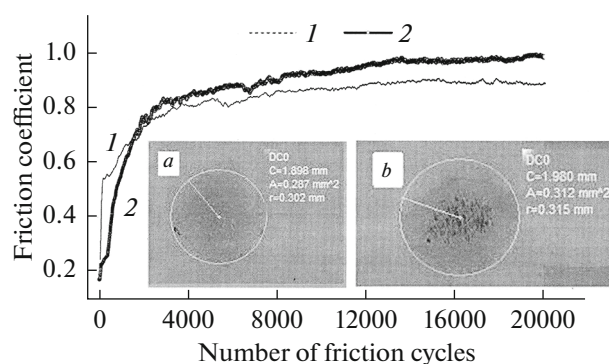


**Fig. 11.** Coefficients of friction depending on the distance traveled for (1) the modified and (2) the initial surface of U10 steel. Inset: images of the wear trace on the surface of the test ball when sliding along (a) the modified and (b) initial surfaces, respectively.

U10 steels on their tribological characteristics, wear tests were carried out, the results of which are shown in Figs. 10 and 11 for U8 and U10 steels, respectively. Measurements were carried out both for the oxidized surface after laser modification and for the surfaces of steels in the initial unirradiated state. Figures 10 and 11 show the dependences of the friction coefficients of a test ball made of corundum ( $\text{Al}_2\text{O}_3$ ) for the modified (curves 1) and initial (curves 2) surfaces of both steel U8 and U10, respectively. The images of the wear trace on the surface of the test ball when sliding on the modified and initial surfaces are demonstrated in insets a and b of these figures.

Some tribological data are given in Table 1; they, together with the data in Figs. 10 and 11, enable evaluation of the effect of oxide layers on the friction process depending on their phase composition.

It is impossible to measure the microhardness of the oxide films directly on the surface of steels due to their small thickness. The available published data [38] on the strength characteristics of individual oxides are presented in Table 2. The lowest hardness values are ascribed to FeO (Table 2), which is adjacent to the unmodified bulk steel, according to the results of XPS analysis. The region of its existence in depth together with iron  $\text{Fe}^0$  in the bulk is approximately twice as large for U8 steel (186.3 nm) than for U10

steel (81.0 nm). For U8 steel, FeO is the main component throughout the entire thickness of the oxidized modified layer. In terms of strength characteristics,  $\text{Fe}_3\text{O}_4$  slightly exceeds FeO (Table 2), but its thickness for U8 steel is small and amounts to 2.7 nm (Fig. 9). Finally, the highest microhardness value is found for  $\text{Fe}_2\text{O}_3$ , which forms the uppermost layer of U8 steel with a thickness of 1.5 nm. The thicknesses of the oxides  $\text{Fe}_2\text{O}_3$  and  $\text{Fe}_3\text{O}_4$  in the case of U10 steel significantly exceed the thicknesses of the corresponding oxides for U8 steel and are in total 81.0 nm (Figs. 8 and 9). Therefore, 4000–5000 friction cycles are sufficient for U8 steel (Fig. 10) for the thin oxide layer to wear out and the coefficient of friction of the modified steel approached its value for unmodified U8 steel. A thicker oxide layer of modified U10 steel, containing  $\text{Fe}_2\text{O}_3$  and  $\text{Fe}_3\text{O}_4$  with better strength characteristics, demonstrates a higher wear resistance than an unirradiated steel surface over 50000 friction cycles (graphs in Figs. 10 and 11 are shown only for 20000 friction cycles).

For U8 steel, the presence of a wustite film on the laser-irradiated surface determines its low wear characteristics. On the contrary, for U10 steel, the wear rate of the modified surface in the presence of  $\text{Fe}_2\text{O}_3$  and  $\text{Fe}_3\text{O}_4$  with higher strength characteristics

**Table 1.** Tribological characteristics of the friction process carried out according to the ball–plane procedure for a corundum ball and the surface of U8 and U10 steels

Steel grade, processing condition	Steel wear rate, $V \times 10^{-10}$ , $\text{mm}^3/\text{N m}$	Ball wear rate, $V \times 10^{-10}$ , $\text{mm}^3/\text{N m}$	Area of the wear mark on the ball surface, $\text{mm}^2$	Friction coefficient, $\mu$
U8, initial	11.7	3.2	246	0.92
U8, after LP	9.7	2.6	222	0.94
U10, initial	16.9	4.4	312	0.92
U10, after LP	7.10	5.2	287	0.88

**Table 2.** Strength characteristics of iron oxides [38]

Oxide, formula, mineral	Hardness on the mineralogical scale	Microhardness	
		microhardness, MPa	load, $P \times 10^{-5}$ , N
FeO, wustite	5.0	5393.85–5398.07	49035–98070
Fe <sub>3</sub> O <sub>4</sub> , magnetite	5.5–6.5	4677.94–7884.83	49035
Fe <sub>2</sub> O <sub>3</sub> , hematite	6.75	10983.84–6864.9	49035

decreases by more than 2 times, while for U8 steel this factor is ~17% (Table 1).

The results indicate that the tribomechanical characteristics and wear dynamics of the modified surface are significantly affected by the oxide layer on the laser-irradiated surface, which has a complex structure over depth, and its structure determines the wear characteristics of the modified surface.

Heating the surface of steels by laser radiation in air, in addition to oxidizing processes, initiates diffusion processes in the surface layers, leading to austenitization with complete dissolution of the carbide phase, and at the cooling stage, it causes quenching with the formation of martensite and residual austenite. In the quenching zone, the microhardness exceeds the microhardness of the base metal by 40–45%; therefore, we can assume that the tribological characteristics of a steel surface after laser processing are determined by the joint effect of both oxide films and the structurally modified zone. Depending on the loading conditions, the prevailing effect on wear is exerted by one or another structural component of the laser-irradiated zone.

## CONCLUSIONS

We study the structure and phase composition of oxide films on carbon tool steels U8 and U10. The depth distribution of the phase components of the oxide layer and their effect on the wear characteristics of the surface during its modification in air are determined. The result of the experiments are the following:

(1) We showed by XPS with ion etching that oxide films on the laser-irradiated surface of both samples of steel have a qualitatively identical layered structure, but there are quantitative differences in the thicknesses of individual phase layers.

(2) We found that the phase components of the oxide films are located in the direction from the base metal to the surface in the following sequence: the layer containing FeO and iron atoms is located deepest, followed by an oxide layer of the composition Fe<sub>3</sub>O<sub>4</sub> and, finally, the outer layer, mainly consisting of a mixture of FeO and Fe<sub>2</sub>O<sub>3</sub>. The thicknesses of completely oxidized surface layers in U8 and U10 steels are ~38.7 and 99.0 nm, respectively. The total thickness of the oxide layer together with the transition

layer of FeO and Fe-Me iron atoms is 20% greater for U8 steel than for U10 steel and is 225.0 nm.

(3) It was found that for U8 steel, the surface film of wustite (FeO) with a thickness of 34.5 nm determines the low wear characteristics of the laser-irradiated surface. On the contrary, a thicker oxide layer of modified U10 steel, containing Fe<sub>2</sub>O<sub>3</sub> and Fe<sub>3</sub>O<sub>4</sub> with better strength characteristics, ensures a higher wear resistance of U10 steel after laser processing. For the modified surface of U10 steel, the wear rate decreases more than twofold, while for U8 steel, this factor is only 17%.

(4) We showed that the tribological properties of the steel surface after laser processing are determined by the combined effect of both oxide films and the structurally modified zone. The presence of wear-resistant structural components after laser processing leads to an increase in the deformation characteristics of steels.

## FUNDING

The research was supported by the Southern Federal University (Internal grant of the Southern Federal University for the implementation of scientific research project no. VnGr-07/2020-01-IF).

## REFERENCES

1. J. F. Ready, D. F. Farson, and T. Feeley, *LIA Handbook of Laser Materials Processing* (Springer, Berlin, 2001).
2. W. M. Steen and J. Mazumder, *Laser Material Processing* (Springer, London, 2010).
3. A. T. Kozakov, S. I. Yares'ko, and A. V. Sidashov, *Modification and Analysis of the Surface of Steels and Alloys* (Rostov. Gos. Univ. Putei Soobshch., Rostov-on-Don, 2015) [in Russian].
4. A. G. Grigor'yants, I. N. Shiganov, and A. I. Misuyurov, *Technological Processes of Laser Processing: Textbook for Universities*, Ed. by A. G. Grigor'yants (Mosk. Gos. Tekh. Univ. im. N.E. Bauman, Moscow, 2006) [in Russian].
5. B. Mao, A. Siddaiah, Y. Liao, and P. L. Menezes, *J. Manuf. Process* **53**, 153 (2020). <https://doi.org/10.1016/j.jmapro.2020.02.009>
6. S. P. Murzin and V. B. Balyakin, *Opt. Laser Technol.* **88**, 96 (2017). <https://doi.org/10.1016/j.optlastec.2016.09.007>

7. S. P. Murzin, V. B. Balyakin, A. A. Melnikov, N. N. Vasiliev, and P. I. Lichtner, *Comput. Opt.* **39**, 64 (2015).  
<https://doi.org/10.18287/0134-2452-2015-39-1-64-69>
8. L. M. Vilhena, M. Sedlaček, B. Podgornik, J. Vižintin, A. Babnik, and J. Možina, *Tribol. Int.* **42**, 1496 (2009).  
<https://doi.org/10.1016/j.triboint.2009.06.003>
9. S. M. Shariff, S. Koppoju, T. K. Pal, P. Gadhe, and S. V. Joshi, *Mater. Sci. Appl.* **6**, 889 (2015).  
<https://doi.org/10.4236/msa.2015.610091>
10. F. V. Bunkin, N. A. Kirichenko, and B. S. Luk'yanchuk, *Phys.—Usp.* **25**, 662 (1982).  
<https://doi.org/10.1070/PU1982v025n09ABEH004601>
11. A. M. Prokhorov, V. I. Konov, I. Ursu, and I. N. Mikheilesku, *Interaction of Laser Radiation with Metals* (Nauka, Moscow, 1988; Academiei, Bukharest, 1988).
12. N. V. Karlov, N. A. Kirichenko, and B. S. Luk'yanchuk, *Lazernaya termokhimiya: uchebnoe rukovodstvo* (TsentrKom, Moscow, 1995) [in Russian].
13. A. A. Uglov, A. A. Volkov, O. G. Sagdedinov, and Yu. Yu. Krivonogov, *J. Eng. Phys.* **58**, 278 (1990).  
<https://doi.org/10.1007/BF00871453>
14. C. Y. Cui, X. G. Cui, X. D. Ren, M. J. Qi, J. D. Hu, and Y. M. Wang, *Appl. Surf. Sci.* **305**, 817 (2014).  
<https://doi.org/10.1016/j.apsusc.2014.04.025>
15. A. T. Kozakov and S. I. Yaresko, *Inorg. Mater.: Appl. Res.* **2**, 254 (2011).  
<https://doi.org/10.1134/S2075113311030130>
16. A. T. Kozakov, S. I. Yares'ko, V. I. Kolesnikov, and A. V. Sidashov, *J. Surf. Invest.: X-Ray, Synchrotron Neutron Tech.* **5**, 431 (2011).  
<https://doi.org/10.1134/S1027451011050089>
17. J. Yang, J. Lian, H. Bai, W. Cui, and Z. Guo, *ISIJ Int.* **45**, 730 (2005).  
<https://doi.org/10.2355/isijinternational.45.730>
18. J. Lian, Q. Dong, Z. Guo, Q. Xu, J. Yang, J. Hu, Q. Guan, and B. Chen, *Mater. Sci. Eng., A* **391**, 210 (2005).  
<https://doi.org/10.1016/j.msea.2004.08.077>
19. Y. H. Liu, J. D. Hu, L. Zhao, Z. X. Guo, A. N. Chumakov, and N. A. Bosak, *Opt. Laser Technol.* **42**, 647 (2010).  
<https://doi.org/10.1016/j.optlastec.2009.11.004>
20. C. Y. Cui, X. G. Cui, Q. Zhao, J. D. Hu, Y. H. Liu, and Y. M. Wang, *Opt. Laser Technol.* **44**, 815 (2012).  
<https://doi.org/10.1016/j.optlastec.2011.11.025>
21. S. I. Yares'ko, *J. Eng. Phys. Thermophys.* **87**, 253 (2014).  
<https://doi.org/10.1007/s10891-014-1008-2>
22. A. M. Bonch-Bruevich and M. N. Libenson, *Izv. Akad. Nauk SSSR, Ser. Fiz.* **46**, 1104 (1982).
23. M. I. Arzuov et al., Preprint No. 152 FIAN (Lebedev Physical Institute, Russian Academy of Sciences, Moscow, 1977).
24. T. F. J. Quinn, *Br. J. Appl. Phys.* **13**, 33 (1962).  
<https://doi.org/10.1088/0508-3443/13/1/308>
25. S. B. Sakrani and J. L. Sullivan, *Proc. SPIE.* **3175**, 176 (1998).  
<https://doi.org/10.1117/12.300662>
26. K. B. Usmanov and G. I. Yakunin, *Effect of the Environments on Wear and Durability of Cutting Tools* (Fan, Tashkent, 1984) [in Russian].
27. I. M. Lyubarskii and L. S. Palatnik, *Metal Physics of Friction* (Metallurgiya, Moscow, 1976) [in Russian].
28. S. L. Yares'ko, *Uprochnyayushchie Tekhnol. Pokrytiya*, No. **3**, 40 (2009).
29. L. G. Korshunov, A. V. Makarov, and L. A. Osintseva, *Trenie Iznos* **9**, 52 (1988).
30. A. V. Makarov, L. G. Korshunov, and L. A. Osintseva, *Trenie Iznos* **12**, 870 (1991).
31. E. Ohmura, Y. Takamachi, and K. Inoue, *Trans. Jpn. Soc. Mech. Eng., A* **56**, 1496 (1990).
32. A. T. Kozakov, A. G. Kochur, K. A. Googlev, A. V. Nikolsky, I. P. Raevskii, V. G. Smotrakov, V. V. Yermkin, *J. Electron Spectrosc. Relat Phenom.* **184**, 16 (2011).  
<https://doi.org/10.1016/j.elspec.2010.10.004>
33. *Practical Surface Analysis by Auger and X-ray Photoelectron Spectroscopy*, Ed. by D. Briggs and M. Seah (Wiley, New York, 1983).
34. V. I. Nefedov, *X-Ray Electron Spectroscopy of Chemical Compounds* (Khimiya, Moscow, 1984) [in Russian].
35. T. Yamashita and P. Hayes, *Appl. Surf. Sci.* **254**, 2441 (2008).  
<https://doi.org/10.1016/j.apsusc.2007.09.063>
36. O. Kubaschewski and B. E. Hopkins, *Oxidation of Metals and Alloys* (Butterworths, London, 1953; Metallurgiya, Moscow, 1965).
37. D. T. Alimov, V. A. Bobyrev, F. V. Bunkin, N. A. Kirichenko, B. S. Luk'yanchuk, Yu. N. Mitin, A. I. Omel'chenko, A. V. Simakin, and P. K. Khabibulaev, *Dokl. Akad. Nauk SSSR*, **268**, 850 (1983).
38. *Physicochemical Properties of Oxides: A Handbook*, Ed. by G. V. Samsonova (Metallurgiya, Moscow, 1978) [in Russian].

Translated by O. Zhukova